JEM Journal of Experimental Medicine

BRIEF DEFINITIVE REPORT

The endothelial basement membrane acts as a checkpoint for entry of pathogenic T cells into the brain

Xueli Zhang[1,2*], Ying Wang[1*], Jian Song[1,2*], Hanna Gerwien[1,2], Omar Chuquisana[1,2], Anna Chashchina[1,2], Cornelia Denz[2,3], and Lydia Sorokin[1,2]

The endothelial cell basement membrane (BM) is a barrier to migrating leukocytes and a rich source of signaling molecules that can influence extravasating cells. Using mice lacking the major endothelial BM components, laminin 411 or 511, in murine experimental autoimmune encephalomyelitis (EAE), we show here that loss of endothelial laminin 511 results in enhanced disease severity due to increased T cell infiltration and altered polarization and pathogenicity of infiltrating T cells. In vitro adhesion and migration assays reveal higher binding to laminin 511 than laminin 411 but faster migration across laminin 411. In vivo and in vitro analyses suggest that integrin α6β1- and αvβ1-mediated binding to laminin 511–high sites not only holds T cells at such sites but also limits their differentiation to pathogenic Th17 cells. This highlights the importance of the interface between the endothelial monolayer and the underlying BM for modulation of immune cell phenotype.

Introduction

The basement membrane (BM) of the endothelium is critical for its barrier function but is frequently overlooked in studies of leukocyte extravasation and vascular permeability. Yet genetic diseases and gene elimination studies provide ample evidence for an instructive role of, in particular, the laminin constituents of BMs in the integrity of barriers (Funk et al., 2018; Nyström and Bruckner-Tuderman, 2019).

Laminins are heterotrimers, composed of α, β, and γ chains that are integral constituents of the BM network (Hohenester and Yurchenco, 2013); 5α, 3β, and 3γ chains combine to form ≤16 different isoforms (Durbeej, 2010). Laminins signal through mainly β1- but also β3- and β4-integrins (Lee et al., 1992; Niessen et al., 1994; Nishiuchi et al., 2006; Tözeren et al., 1994); however, there are comparatively little data on laminin signaling in immune cells (García-Nieto et al., 2010; Milner and Campbell, 2002; Schöttelndreier et al., 2001; Shaw et al., 1990). Laminin α4 and α5 chains predominate in endothelial BMs, where they combine with β1 and γ1 chains to form laminins 411 and 511 (Frieser et al., 1997; Sorokin et al., 1997), the expression of which varies along the vascular tree. Sites of laminin 411 and 511 co-localization alternate with sites of little or no laminin 511 at postcapillary venules, where leukocyte extravasation predominantly occurs (Sixt et al., 2001a; Song et al., 2017; Wang et al., 2006; Wu et al., 2009). In vitro assays have shown that laminin 511 and 411 support the adhesion and 2D migration of different leukocyte types; however, differences have been reported for T cells and neutrophils (Song et al., 2017; Sixt et al., 2001a; Wu et al., 2009), and precisely how laminins affect leukocyte infiltration into inflamed tissues is unclear. Recent intravital studies revealed that extravasating leukocytes take 3–4 min to penetrate the endothelial monolayer and migrate beneath the endothelial monolayer for ≤30 min before they finally penetrate the endothelial BM (Song et al., 2017; Woodfin et al., 2011). This highlights the barrier function of the BM and raises the question of whether signals from the subendothelial site affect other processes required for finalBM penetration.

We use here a T cell–induced neuroinflammatory model, experimental autoimmune encephalomyelitis (EAE), and mice lacking endothelial laminin 511 (*Tek-cre::Lama5*$^{-/-}$; Di Russo et al., 2017) or laminin 411 (*Lama4*$^{-/-}$; Thyboll et al., 2002) to address how the endothelial laminins affected T cell behavior and disease induction. In the brain, the barrier function of vessels is particularly important to protect sensitive neurons from blood-borne pathogens and toxins, and specialized

[1]Institute of Physiological Chemistry and Pathobiochemistry, University of Muenster, Muenster, Germany; [2]Cells-in-Motion Cluster of Excellence, University of Muenster, Muenster, Germany; [3]Institute of Applied Physics, University of Muenster, Muenster, Germany.

*X. Zhang, Y. Wang, and J. Song contributed equally to this paper; Correspondence to Lydia Sorokin: sorokin@uni-muenster.de; X. Zhang's present address is State Key Laboratory of Oncogenes and Related Genes, Shanghai Cancer Institute, Ren Ji Hospital, School of Medicine, Shanghai Jiao Tong University, Shanghai, China; Y. Wang's present address is Institute of Health Sciences, Shanghai Institutes for Biological Sciences/Shanghai Jiao Tong University, Shanghai, China.

mechanisms exist to enhance endothelial barrier properties. These include complex tight junctions between endothelial cells and, in addition to the endothelial BM, an astroglial layer and associated BM (Sorokin, 2010). This unique double-BM structure of cerebral vessels (Sixt et al., 2001a) permits precise localization of sites of leukocyte extravasation. In addition, the EAE model permits isolation of the disease-inducing primary CD4$^+$ T lymphocytes for in vitro and in vivo competitive migration assays and pathogenicity analyses. We demonstrate that differential expression of integrins α6β1 and αvβ1 on circulating encephalitogenic T cells defines their ability to interact with endothelial laminins 511 and 411, which in turn modulates T cell motility but also polarization toward a pathogenic T helper 17 (Th17) population, which we hypothesize affects the extent of central nervous system (CNS) infiltration and EAE severity. Our data identify a new niche beneath the endothelial monolayer at the endothelial BM as an important site for modulation of the phenotype of immune cells on route into inflamed tissues.

Results and discussion

To investigate T cell binding and migration on the endothelial laminins, in vitro assays were performed with primary encephalitogenic CD4$^+$ T cells obtained from WT mice at peak EAE. In vitro adhesion assays revealed high-level and time-dependent adhesion of encephalitogenic T cells to laminin 511 and to the control substrate, VCAM-1, and low binding to laminin 411 and laminin 111, a control nonendothelial laminin (Fig. 1 A). Optical tweezers experiments, performed at 70 pN to detach cells, permitted measurement of the strength of T cell adhesion to low (0.1 µg/ml) or high (1 µg/ml) concentrations of laminin 411 or 511. The distance the cells could be stretched before detachment was inversely correlated to the strength of adhesion, revealing no detachment from either low or high concentrations of laminin 511 (Fig. 1 B), indicating exceptionally strong adhesion strength. This correlated with a significantly reduced extent and speed of 2D chemotaxis of encephalitogenic CD4$^+$ T cells on laminin 511 compared with laminin 411 (Fig. 1, C and D), consistent with the reduced transmigration across laminin 511 compared with laminin 411 that we have previously reported (Wu et al., 2009). The same pattern of results was obtained with Th1 and Th17 cells, Th populations critical in EAE, which did not differ in their ability to bind to laminin 511 and 411 (Fig. 1 E).

To identify the receptors mediating adhesion and migration of T cells on laminins 511 and 411, adhesion assays were performed in the presence of function blocking antibodies to the main laminin-binding integrins expressed on T cells, integrins α6, β1, and β3 (Wu et al., 2009), or in the presence of arginyl-glycylaspartic acid (RGD) peptides that block αv-integrins (Pallarola et al., 2014). Adhesion to laminin 411 was reduced to 50–60% in the presence of antibodies to integrin α6 or β1, whereas anti-integrin β3 had no effect (Fig. 2 A), excluding αvβ3 and suggesting the involvement of α6β1 plus a nonintegrin receptor, as implied by the lack of complete inhibition of binding by any of the anti-integrin antibodies. Binding to laminin 511 was reduced to 45% by anti-integrin β1 and 55% by anti-integrin α6, suggesting involvement of integrin α6β1 and an additional β1 integrin (Fig. 2 B); anti-integrin β3 antibody had no effect (Fig. 2 B). Because of limitations in the availability of function-blocking antibodies to murine integrin α chains, we used linear RGD to characterize the integrins binding to laminin 511. At 10 µM, linear RGD inhibits only αvβ1, and at 100 µM, αvβ1 and α5β1 are inhibited (Sasaki and Timpl, 2001; Sixt et al., 2001b). 10 µM and 100 µM RGD showed the same 40–45% inhibition of T cell adhesion to laminin 511 (Fig. 2 B), suggesting the involvement of αvβ1 and not α5β1. Hence, integrin α6β1 plus a nonintegrin receptor, probably MCAM-1, supports binding to laminin 411 (Flanagan et al., 2012), and α6β1 and αvβ1 are required for strong T cell adhesion to laminin 511. Although integrin αvβ3 has been shown to be expressed by encephalitogenic T cells (Du et al., 2016) and to be involved in T cell migration on interstitial matrix molecules, such as vitronectin and fibronectin (Overstreet et al., 2013), it is not required for binding to laminin 511.

We have previously shown reduced EAE severity in bone marrow chimeric mice carrying *Itga6*$^{-/-}$ bone marrow (Wu et al., 2009). We here used *Itga6*$^{-/-}$ T cells from such chimeric mice and *Itgav*$^{-/-}$ T cells from *CD4-cre::Itgav*$^{-/-}$ mice at peak EAE for in vitro adhesion and migration assays. Flow cytometry of *Itga6*$^{-/-}$ and *Itgav*$^{-/-}$ T cells revealed no difference from WT controls in the expression of other integrins (Fig. S1, A and B), nor did EAE affect expression levels of integrins α6, αv, and β1 on T cells (Fig. S1 C). The binding of *Itga6*$^{-/-}$ cells to laminin 411 and of *Itgav*$^{-/-}$ and *Itga6*$^{-/-}$ T cells to laminin 511 were significantly reduced compared with WT cells (Fig. 2 C). Function blocking antibody to integrin α6 ablated the binding of *Itgav*$^{-/-}$ T cells to laminin 511 (Fig. 2 C). This suggests that integrins α6β1 and αvβ1 are required for binding to laminin 511 and do not compensate for each other, and therefore probably signal different information.

To distinguish between integrin α6β1– and αvβ1–induced effects, we used recombinant laminin 511 domain IVa (Sasaki and Timpl, 2001) and mini-laminin 511 (Künneken et al., 2004), which carry only αvβ1 or α6β1 binding sites, respectively. Both domain IVa and mini-laminin 511 supported concentration-dependent, saturable binding of WT encephalitogenic T cells, indicative of receptor-mediated binding (Fig. S2 A). As expected, *Itgav*$^{-/-}$ T cells showed no binding to laminin 511 domain IVa, whereas binding of *Itga6*$^{-/-}$ T cells was comparable to that of WT cells (Fig. 2 D). Conversely, *Itga6*$^{-/-}$ T cells did not bind to mini-laminin 511, and binding of *Itgav*$^{-/-}$ T cells was not affected unless they were preincubated with anti-integrin α6β1 (Fig. 2 D).

In chemotaxis assays, both mini-laminin 511 and domain IVa showed reduced capacity to support transmigration of T cells compared with laminin 411 (Fig. S2 B). Surprisingly, *Itgav*$^{-/-}$ T cells showed enhanced chemotaxis across domain IVa, whereas *Itga6*$^{-/-}$ T cells showed no difference from WT cells in migration across mini-laminin 511 or domain IVa (Fig. 2 E). This suggests that αvβ1-mediated binding to the domain IVa of laminin α5 inhibits T cell migration, and that integrin α6β1 binding to C-terminal domains of laminin 511, while permissive, does not promote migration. By contrast, *Itga6*$^{-/-}$ T cells showed

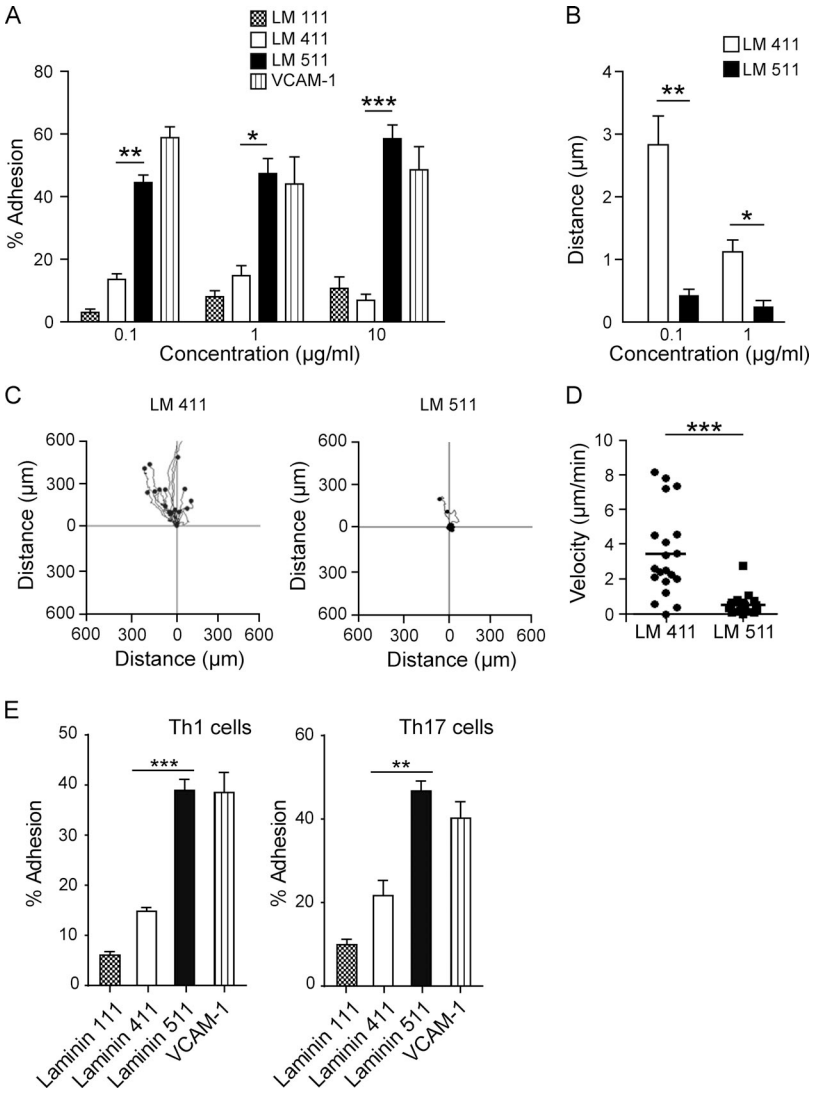

Figure 1. **Primary encephalitogenic CD4⁺ T cells show high affinity binding but low migration on laminin 511.** **(A)** Binding of encephalitogenic CD4⁺ T cells to laminins 411 and 511, nonendothelial laminin 111, and the positive control VCAM-1. Data are means ± SD of six experiments, *n* = 3 mice/experiment and three to four replicates/group. Statistical analysis used a Mann–Whitney *U* test; *, P < 0.05; **, P < 0.01; ***, P < 0.001. **(B)** Optical tweezer experiments showing displacement distance of CD4⁺ T cells plated on high and low concentrations of laminin 411 or 511 under 70 pN laser strength. Data are means of three experiments ± SD, *n* = 3 mice/experiment and 10 cells/group. Statistical analysis used a Mann–Whitney *U* test; *, P < 0.05; **, P < 0.01. **(C and D)** Representative migration trajectories of CD4⁺ T cells on laminin 411 or 511 in response to CCL21 (C) and corresponding mean velocities of all cells measured (D); two independent experiments were performed, *n* = 3 mice/experiment and 20 cells/group. Statistical analysis used a Mann–Whitney *U* test; ***, P < 0.001. **(E)** Binding of encephalitogenic Th1 and Th17 cells to 10 µg/ml laminins 411, 511, and 111 and VCAM-1. Data are means of six experiments ± SD, *n* = 3 mice/experiment and three to four replicates/group. Statistical analysis used a Mann–Whitney *U* test; **, P < 0.01; ***, P < 0.001.

significantly reduced migration across laminin 411 (Fig. 2 E), suggesting that integrin α6β1 promotes migration across laminin 411.

CD4-cre::Itgav$^{-/-}$ mice have previously been used in EAE (Acharya et al., 2010), revealing mild effects that include a slightly faster induction and higher peak severity, consistent with faster leukocyte infiltration into the brain. However, as high doses of 35–55 peptide of myelin oligodendrocyte glycoprotein (MOG_{35-55}) promote strong myeloid infiltration that contributes to disease severity and can mask the effects of the early infiltrating disease-inducing T cells (Croxford et al., 2015; Tran et al., 1998), we directly compared the migration capacity of integrin αv–positive and –negative encephalitogenic T cells in in vivo competitive migration assays. A 1:1 ratio of 6-carboxytetramethylrhodamine (TAMRA)⁺ *Itgav*$^{-/-}$:CFSE⁺ WT CD4⁺ encephalitogenic T cells was transferred into WT EAE recipients, and the number of donor cells in brains was quantified by flow cytometry. A significantly higher proportion of *Itgav*$^{-/-}$ compared with WT CD4⁺ T cells was measured in brains of host EAE mice 24 h after transfer (Fig. 2, F and G), indicating faster in vivo migration of T cells lacking integrin αvβ1 and consistent with faster penetration of the endothelial BM. Corresponding immunofluorescence staining of the brains confirmed a larger proportion of the red TAMRA⁺ *Itgav*$^{-/-}$ cells associated with perivascular cuffs compared with the green CSFE⁺ WT cells, whereas both cells were present in equal proportions in lymph nodes (Fig. 2, H and I).

To investigate whether the levels of integrins α6β1 and αvβ1 on CD4 T cells in the periphery (lymph node and spleen) differed from those infiltrating the brain, flow cytometry was performed on WT mice at peak EAE. In general, α6β1 and αvβ1 levels in T cells were not altered in EAE compared with naive conditions in the periphery (Fig. S1 C). Equal proportions of integrin α6β1–high and –low cells occurred in the periphery, a small proportion of which also expressed integrin αvβ1 (Fig. 3, A and B). In the brain, however, >90% cells were $\alpha 6^{high}$, and of these cells, ∼65% were integrin αv^{high} (Fig. 3, A and B). As integrin αv has been identified as a negative regulator of pathogenicity in single-cell RNA analyses of Th17 cells in EAE (Gaublomme et al., 2015), we used real-time quantitative PCR (qPCR) to analyze markers of pathogenic encephalitogenic Th17 cells in these two populations. qPCR revealed 2–20-fold higher expression of *Plzp*,

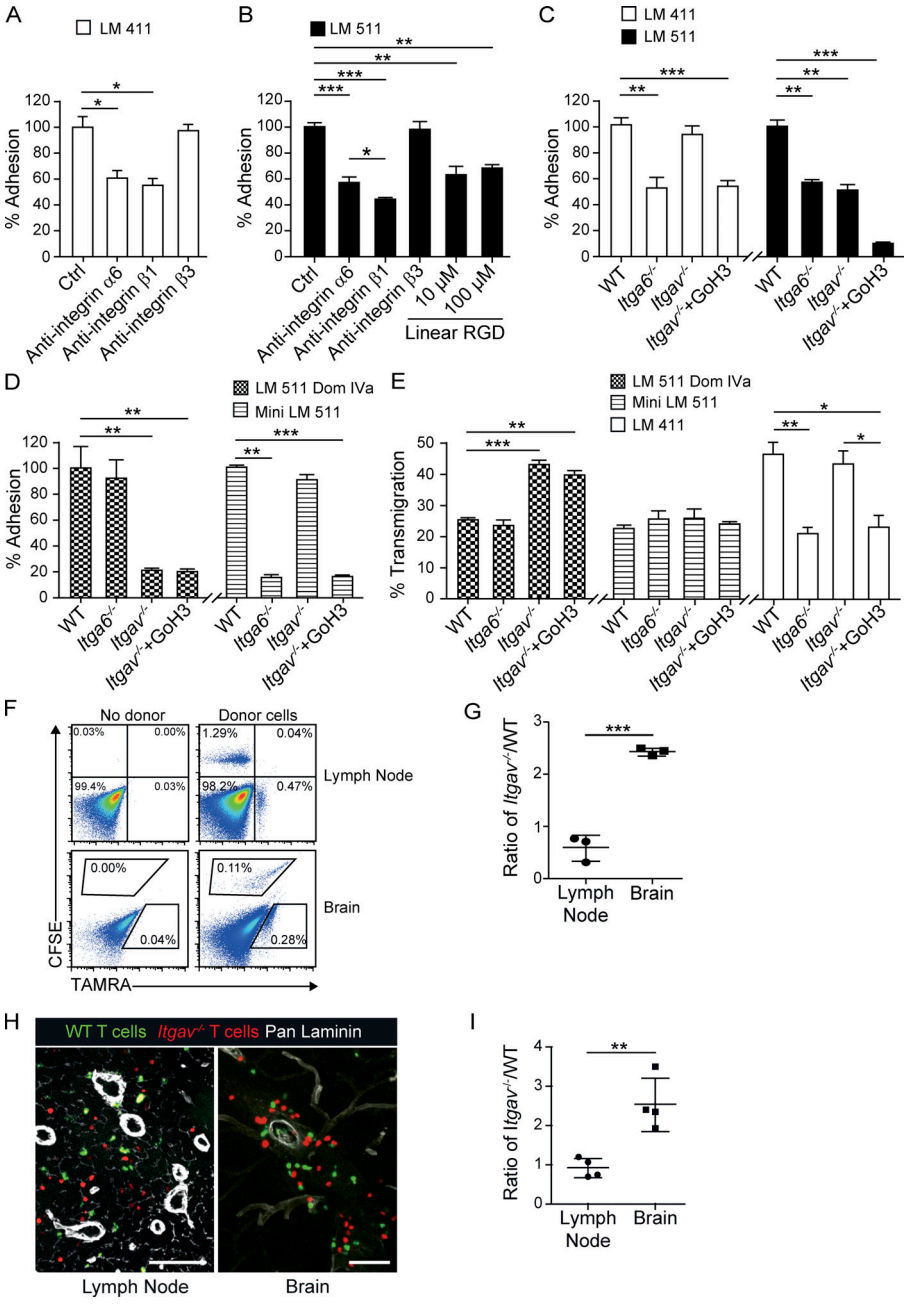

Figure 2. **Integrins α6β1 and αvβ1 mediate encephalitogenic CD4⁺ T cell adhesion and migration across endothelial laminins. (A and B)** WT CD4⁺ T cell adhesion to laminins 411 (A) or 511 (B) in the presence or absence of function blocking antibodies to integrins α6 (GoH3), β1 (Ha/5), or β3 (2C9.G2) or high and low concentrations of linear RGD. Data are percentage of total cells added; means ± SD of six experiments are shown, *n* = 3 mice/experiment and five replicates/group. Statistical analysis used a Mann–Whitney *U* test; *, P < 0.05; **, P < 0.01; ***, P < 0.001. **(C and D)** Binding of WT, *Itga6*$^{-/-}$, or *Itgav*$^{-/-}$ CD4⁺ T cells to laminin 411 or 511 (C) and mini-laminin 511 or laminin 511 domain IVa (D). Data are percentage binding relative to binding in the absence of blocking agents or to WT cells; means ± SD of six experiments are shown, *n* = 3 mice/experiment and three to four replicates/group. Statistical analysis used a Mann–Whitney *U* test; **, P < 0.01; ***, P < 0.001. **(E)** Chemotaxis of WT, *Itga6*$^{-/-}$, or *Itgav*$^{-/-}$ CD4⁺ T cells across mini-laminin 511, laminin 511 domain IVa, or laminin 411. Data are percentage of total cells added; means ± SD of six experiments are shown, *n* = 3 mice/experiment and three to four replicates/group. Statistical analysis used a Mann–Whitney *U* test; *, P < 0.05; **, P < 0.01; ***, P < 0.001. **(F and G)** Representative flow cytometry of TAMRA⁺ *Itgav*$^{-/-}$ and CFSE⁺ WT CD4⁺ T cells in WT hosts 24 h after transfer (F) and corresponding quantification of *Itgav*$^{-/-}$ relative to WT cells (G). Data are values from three independent experiments with *n* = 3–4 mice/group/experiment; mean values ± SD are shown. Statistical analysis used a Mann–Whitney *U* test; ***, P < 0.001. **(H and I)** Representative immunofluorescence staining of TAMRA⁺ *Itgav*$^{-/-}$ and CFSE⁺ WT CD4⁺ T cells in WT lymph nodes and brains (scale bar = 50 µm; H) and quantification of the data from at least five sections/organ/host and four to five hosts (I). Data are means ± SD; statistical analysis was done by a Mann–Whitney *U* test; **, P < 0.01.

Il17a, *Ifng*, and *Gpr65*, and reduced expression of *Cd5l* in integrin α6^{high}αv^{low} cells compared with integrin α6^{high}αv^{high} cells (Fig. 3 C), suggesting that they represent a T cell population with higher pathogenicity (Gaublomme et al., 2015; Wang et al., 2015) and raising the question whether laminins in the endothelial BM of postcapillary venules modulate the phenotype of the infiltrating cells.

EAE-derived CD4⁺ T cells were, therefore, cultured on laminin 411, laminin 511, or no coating and differentiated to Th1 or Th17 cells (Seder et al., 1993; Veldhoen et al., 2006). This revealed reduced Th1 and Th17 differentiation of cells on laminin 511 compared with laminin 411 or no laminin (Fig. 3, D and E). qPCR for pathogenic markers also revealed reduced expression of *Ifng* and *Il17a* as well as several other pathogenic markers including *Plzp*, *Il23r*, and *Gpr65*, but not *Il10* in the Th17 cells on laminin 511 (Fig. 3 F). This is suggestive of a mixed Th1/Th17 phenotype of low pathogenicity identified in the CNS of EAE mice by single-cell RNA analyses (Gaublomme et al., 2015). Taken together, the data suggest that high-affinity integrin α6β1- and αvβ1-mediated binding of T cells to laminin 511 in the endothelial BM limits transmigration and differentiation to pathogenic Th17 cells, thereby limiting the entry of disease-inducing cells and EAE severity.

Hence, mice lacking laminin α5 in endothelial BMs should exhibit higher EAE severity. Indeed, *Tek-cre::Lama5*$^{-/-}$ mice, which lack laminin α5 in endothelial BMs only (Di Russo et al., 2017), exhibited significantly higher disease severity and mortality than WT littermates, when EAE was induced with both (normal) high- or low-dose MOG_{35-55} (to minimize lethality;

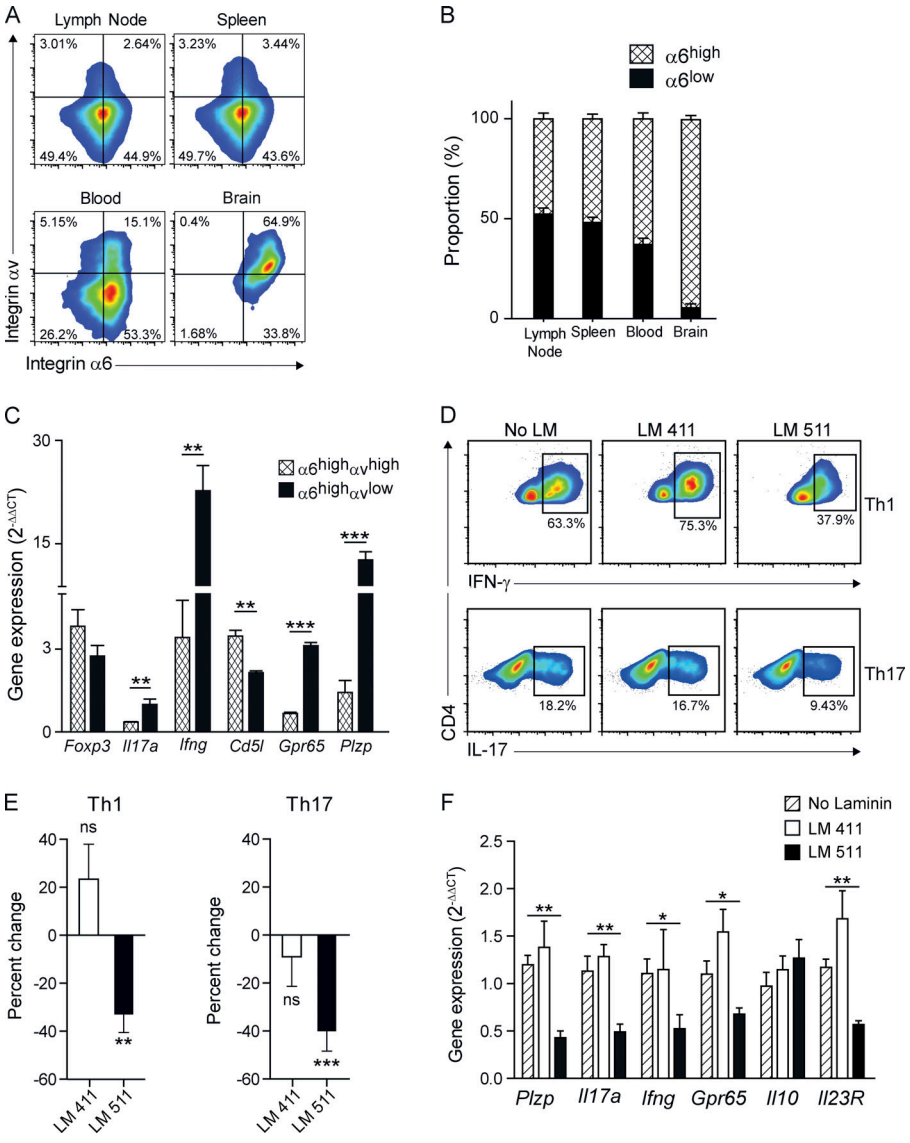

Figure 3. **Integrin α6^{high}αv^{low} marks pathogenic Th17 cells, the differentiation of which is altered by endothelial laminins. (A and B)** Representative flow cytometry of integrins α6 and αv on CD4$^+$ T cells in the blood, lymph nodes, spleens, and brains of WT mice at peak EAE (A), and corresponding quantification of integrin α6–high and –low populations (B). Data are means ± SD of three experiments, *n* = 3 mice/group/experiment. Statistical analysis used a Mann–Whitney *U* test. **(C)** qPCR for the regulatory T cell marker, *Foxp3*, and Th17 pathogenicity markers in integrin α6^{high}αv^{high} and α6^{high}αv^{low} CD4$^+$ T cells isolated from brains of WT mice at peak EAE. Data are means ± SD of four experiments, *n* = 3–6 mice/experiment and triplicates/group. Statistical analysis used a Mann–Whitney *U* test; **, P < 0.01; ***, P < 0.001. **(D and E)** Representative flow cytometry for CD4 and IFN-γ or IL-17 to identify Th1 and Th17 cells derived from in vitro differentiated MOG-specific CD4$^+$ T cells cultured on laminin 411, laminin 511, or no coating (D), and corresponding quantification of the data expressed as percentage change from cells plated on uncoated plastic (E). Data are means ± SD of four experiments, *n* = 3–6 mice/experiment and triplicates/group. Statistical analysis used a Mann–Whitney *U* test; **, P < 0.01; ***, P < 0.001. **(F)** Corresponding qPCR for pathogenicity markers in Th17 cells performed in two experiments. Data are means ± SD, *n* = 4 mice/experiment with triplicates/group. Statistical analysis used a Mann–Whitney *U* test; *, P < 0.05; **, P < 0.01.

Fig. 4, A–E). This was associated with elevated numbers of CD4$^+$ T lymphocytes, CD11b$^+$ macrophages, and Th1 and Th17 cells in the brains and spinal cords of *Tek-cre::Lama5*$^{-/-}$ mice at peak disease compared with WT littermates (Fig. 4, F and G; and Fig. S3 A). However, numbers of CD4$^+$ and CD8$^+$ T cells, B220$^+$ B cells, CD11b$^+$ macrophages, and Th1 and Th17 cells in lymph nodes and in the circulation were not altered in *Tek-cre::Lama5*$^{-/-}$ compared with WT mice (Fig. 4 F). As reliable markers for in vivo staining of Th17 and Th1 cells do not exist, it was not possible to investigate Th1 and Th17 cells in the inflammatory cuffs.

In vivo proliferation assays were performed to check for enhanced proliferation of T cells in the brains of *Tek-cre::Lama5*$^{-/-}$, which could account for the observed high EAE severity and elevated numbers of the disease-inducing CD4$^+$ T cells in these mice. Although more CD4$^+$ T cells were present in the brains of *Tek-cre::Lama5*$^{-/-}$ mice, the proportion of proliferating cells was the same as in WT littermates in brains, lymph nodes, spleen, and blood (Fig. S3 B). However, adoptive transfer of CD45.1$^+$ WT encephalitogenic T cells to CD45.2$^+$ *Tek-cre::Lama5*$^{-/-}$ or WT recipients and measurement of infiltrated CD45.1$^+$ CD4$^+$ T cells at day 3 after transfer, before proliferation of cells is detectable (Bai et al., 2004), revealed faster migration of T cells into the CNS of *Tek-cre::Lama5*$^{-/-}$ mice only (Fig. S3 C) and, long-term, higher disease scores and more extensive CNS T cell infiltration in *Tek-cre::Lama5*$^{-/-}$ mice (Fig. S3, D–F).

Flow cytometry at peak EAE revealed 53–63% integrin α6^{high}αv^{high} T cells in the brains of WT and Tek-cre::*Lama5*$^{-/-}$ mice and 35–45% of the pathogenic α6^{high}αv^{low} population (Fig. 5, A and B). However, this pattern was reversed in *Lama4*$^{-/-}$ brains, in which 60% of T cells exhibited the pathogenic α6^{high}αv^{low} phenotype (Fig. 5, A and B), despite overall lower numbers of infiltrating leukocytes (Fig. 5 C). There were no differences between the three strains in peripheral CD4 T cell populations (Fig. 5 A). *Lama4*$^{-/-}$ mice have an even expression of laminin 511 in all endothelial BMs and exhibit less-severe EAE owing to reduced total CD4 T cell infiltration into the brain (Wu et al., 2009). Taken together, these data suggest that laminin 511–positive endothelial BMs in *Lama4*$^{-/-}$ mice can be penetrated by the pathogenic α6^{high}αv^{low} T cells, explaining why they show EAE symptoms (Wu et al., 2009), and substantiating our in vitro

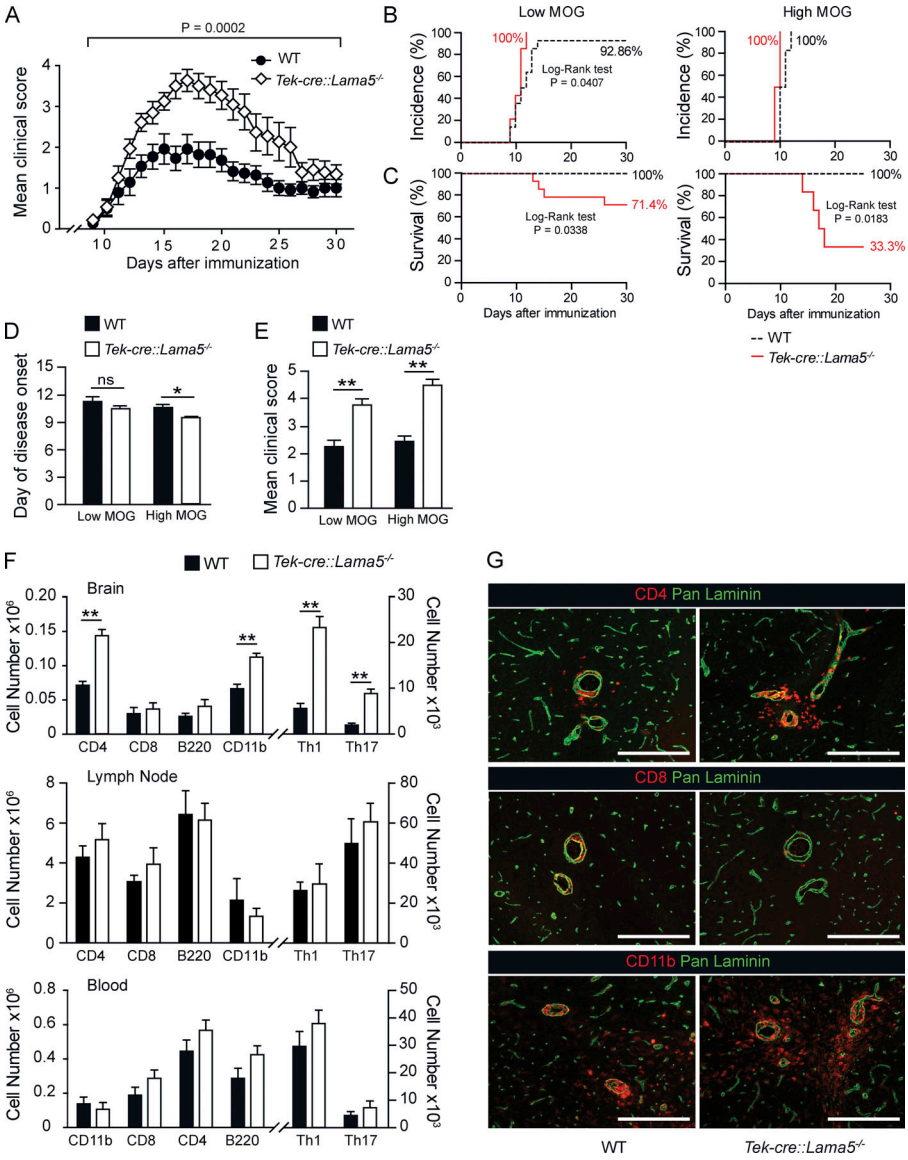

Figure 4. **Increased EAE severity in *Tek-cre::Lama5*$^{-/-}$ mice. (A)** EAE scores versus days after low-dose MOG_{35-55} immunization of *Tek-cre::Lama5*$^{-/-}$ and WT littermates. Data are mean scores ± SD from three experiments, n = 14 mice/group. Statistical analysis used a Mann–Whitney U test; P value is shown. **(B–E)** Corresponding Kaplan–Meier curves showing EAE incidence (B) and survival (C) and bar graphs showing mean day of disease onset (D) and mean clinical scores (E) in mice immunized with high- or low-dose MOG_{35-55}. Statistical tests were log-rank tests; P values in B and C are shown; *, P < 0.05; **, P < 0.01; ns, not significant. **(F)** Flow cytometry quantification of $CD4^+$ and $CD8^+$ T cells, $B220^+$ B cells, $CD11b^+$ macrophages, and Th1 and Th17 $CD4^+$ T cells in brains, lymph nodes, and blood of *Tek-cre::Lama5*$^{-/-}$ and WT littermates at peak disease (day 17). Data are means ± SD of three experiments, n = 15 mice/group. Statistical analysis used a Mann–Whitney U test; **, P < 0.01. **(G)** Corresponding CD4, CD8, and CD11b immunofluorescence stainings; scale bars are 100 µm.

data that integrin αv expression normally inhibits migration across laminin 511. Due to antibody availability, it is impossible to stain for integrin α6-high or -low and integrin αv-high or -low T cells in EAE brain sections in relation to laminin 511 expression levels (Sixt et al., 2001a).

Our data and those of others (Acharya et al., 2010; Gaublomme et al., 2015) suggest that expression of integrin αvβ1 on T cells does not drive EAE, but that its expression level is inversely correlated with pathogenicity, which may act together with other factors, potentially integrin α6β1, to influence T cell differentiation. All T cells entering the CNS showed high integrin α6β1 expression compared with circulating T cells (Fig. S1 C), as reported in other inflammatory situations (Dangerfield et al., 2002), and genetic elimination in immune cells or antibody blocking of integrin α6β1 delays EAE onset and reduces severity (Wu et al., 2009). While α6β1 and αvβ1 act as adhesion receptors for laminin 411 and/or 511 and the strength of adhesion can affect migration across BMs, data from the in vitro Th1 and Th17 differentiation experiments suggest that they can also transduce signals that are independent of migration (Fig. 3, D–F). Laminins affect differentiation of various cells, and there are many examples of genetic diseases caused by laminin mutations and severe phenotypes when specific laminin chains are knocked out in mice (Miner and Yurchenco, 2004; Yurchenco et al., 2018). However, they have not been previously implicated in modulating immune cell phenotypes in inflammation, which we propose occurs at the endothelial BM. This may explain why immune cells migrating into inflamed tissues spend disproportionately long periods at this site before finally penetrating into the tissue (Song et al., 2017; Woodfin et al., 2011), and highlights the subendothelial/BM niche as a critical site for modulating the phenotype of infiltrating cells (Fig. 5 D).

Materials and methods

Mice

Mice used included laminin α5 endothelial cell–specific knockout mice (*Tek-cre::Lama5*$^{-/-}$; Di Russo et al., 2017; Song et al.,

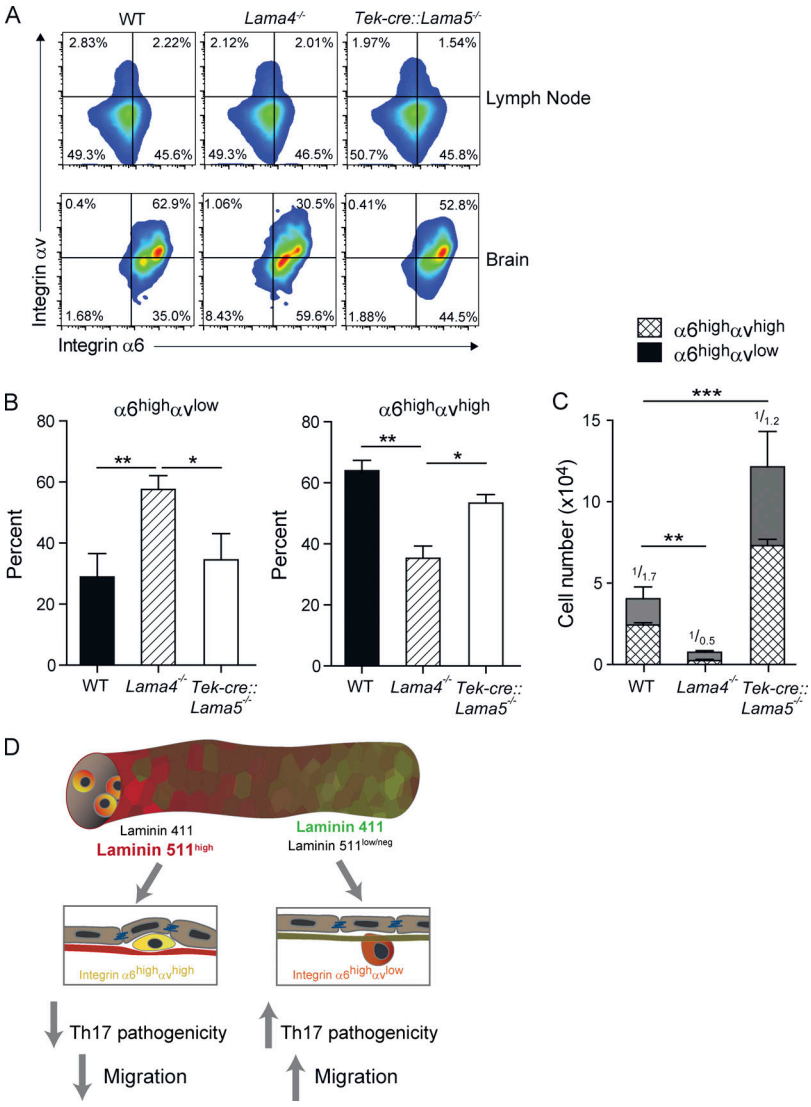

Figure 5. **Integrin α6^{high}αv^{low} CD4$^+$ T cells predominate in brains of *Lama4*$^{-/-}$ mice at peak EAE. (A and B)** Representative flow cytometry of integrins α6 and αv on CD4$^+$ T cells in the periphery (lymph node) and brain (without meninges) of *Lama4*$^{-/-}$, *Tek-cre::Lama5*$^{-/-}$, and WT mice at peak EAE (A) and corresponding quantification of proportions of integrin α6^{high}αv^{high} and α6^{high}αv^{low} T cells (B). **(C)** Total CD4$^+$ T cell infiltrates in *Lama4*$^{-/-}$ and *Tek-cre::Lama5*$^{-/-}$ and WT mice at peak EAE showing ratios of integrin α6^{high}αv^{high} to α6^{high}αv^{low} T cells. Data are means ± SD of four experiments, n = 6 mice/group. Statistical analysis used a Mann–Whitney U test; *, P < 0.05; **, P < 0.01; ***, P < 0.001. **(D)** Scheme showing that laminin 511^{high} sites in the endothelial BM bind extravasating integrin α6^{high}/αv^{high} T cells, restricting their differentiation to the highly motile, pathogenic integrin α6^{high}/αv^{low} Th17 population and, thereby, acting as a checkpoint in neuroinflammation.

2013), laminin α4 knockout mice (*Lama4*$^{-/-}$; Thyboll et al., 2002), T cell–specific integrin αvβ1-null (*CD4-cre::Itgav*$^{-/-}$) mice generated by crossing the *Itgav*$^{floxed/floxed}$ mouse (McCarty et al., 2005) with the CD4-cre strain (Lee et al., 2001), and *Itga6*$^{-/-}$ mice (Georges-Labouesse et al., 1996); all strains were backcrossed ≥16 times onto a C57BL/6 background. WT littermate controls and WT C57BL/6 mice (Charles River) were used as controls for *Lama4*$^{-/-}$ mice, *Lama5*$^{floxed/floxed}$ mice were used as WT controls for *Tek-cre::Lama5*$^{-/-}$ mice, and *Itgav*$^{floxed/floxed}$ cells were designated WT controls for *CD4-cre::Itgav*$^{-/-}$ mice. As *Itga6*$^{floxed/floxed}$ mice are not freely available, and as complete knockouts die perinatally (Georges-Labouesse et al., 1996), it was necessary to generate chimeric mice carrying *Itga6*$^{-/-}$ bone marrow as described previously (Song et al., 2015). WT controls were generated in the same manner, except that C57BL/6 hosts were reconstituted with WT bone marrow (Charles River). WT recipient mice were lethally irradiated with a single dose of 11 Gy and reconstituted by i.v. injection of 10^7 *Itga6*$^{-/-}$ donor fetal liver cells. Animals were analyzed after 6–8 wk by flow cytometry for reconstitution of the hematopoietic system and used in EAE experiments thereafter. CD45.1 versus CD45.2 allelic markers were used to trace donor versus host cells in passive transfer and bone marrow chimera experiments. Animal breeding and all experiments were conducted according to the Landesamt für Natur, Umwelt und Verbraucherschutz Nordrhein-Westfalen, permit numbers 84-02.04.2011.A087 and 84-02.04.2014.A075.

Antibodies, proteins, and inhibitors

The antibodies used in immunofluorescence staining and flow cytometry were laminin α4 (377; Ringelmann et al., 1999), laminin α5 (4G6; Sorokin et al., 1997), laminin γ1 (3E10; Sixt et al., 2001a), pan-laminin (455; Sorokin et al., 1997), CD45 (30G.12), CD45.2 (104, eBioscience), CD45.1 (A20, BD PharMingen), CD11b/MAC-1 (M1/70, BD PharMingen), CD11c (N418, eBioscience), CD4 (H129.19, BD PharMingen), CD8 (53-6.7, eBioscience), B220 (RA3-6B2, BD PharMingen), IL-17 (TC11-18H10.1, BD PharMingen), IFN-γ (XMG1.2, BD PharMingen), integrin β1 (eBioHMb1-1 [HMb1-1], eBioscience), integrin β2 (C71/16, BD PharMingen), integrin β3 (2C9.G2, BD PharMingen), integrin α6 (GoH3, PharMingen), integrin α5 (5H10-27 [MFR5], BD PharMingen), integrin αv (RMV-7, BD PharMingen), MCAM (ME-9F1, Miltenyi Biotec), and integrin α4 (PS/2, BD PharMingen).

Laminin 411 and 511 were purified as previously described (Sixt et al., 2001b). Recombinant laminin α5 domain IVa was produced in HEK293 cells as described previously (Sasaki and Timpl, 2001); mini-laminin 511 composed of the C-terminal sequences of laminin α5, β1, and γ1 chains was from Takara Bio (Künneken et al., 2004; Miyazaki et al., 2008).

Active EAE

EAE was induced using $MOG_{35–55}$ as previously described (Sixt et al., 2001a; Wu et al., 2009). EAE onset was defined as day 10 after immunization and peak EAE as day 14–17 after immunization. EAE was induced in WT, *Tek-cre::Lama5*$^{-/-}$, *CD4-cre::Itgav*$^{-/-}$, and chimeric mice carrying *Itga6*$^{-/-}$ bone marrow. In some experiments performed with *Tek-cre::Lama5*$^{-/-}$ and *CD4-cre::Itgav*$^{-/-}$ mice, it was necessary to use 75 µg $MOG_{35–55}$ (low dose) instead of the standard 112 µg dose (high dose) to reduce EAE severity and mortality.

Passive EAE

Passive transfer of encephalitogenic T cells was as previously described (Wu et al., 2009). Polymorphic lineage determinants (CD45.1 or CD45.2) were used for tracking donor versus host immune cells. For in vivo transmigration assays, the donor cells that transmigrated into the host CNS by day 3 after passive transfer were measured. In some cases, encephalitogenic T cells (5×10^6 cells) were isolated from the lymph nodes of peak EAE mice and labeled with TAMRA for *Itgv*$^{-/-}$ or CFSE for WT cells and transferred i.v. into EAE mice on day 15 after $MOG_{35–55}$ immunization; lymph nodes, spleens, and brains were isolated 24 h after transfer, and TAMRA$^+$/CFSE$^+$ CD4$^+$ T cells were quantified with a FACSCelesta flow cytometer (Becton Dickinson).

Flow cytometry

Mice were perfused with PBS before spleens, lymph nodes, and CNS were harvested; the meninges were removed from brains, and cells were isolated from all tissues by cell straining (70 µm for spleens and lymph nodes, 100 µm for CNS). For spleen cells, erythrocytes were lysed by incubating the cells on ice for 3 min with lysing buffer (BD Pharm Lyse); leukocytes from blood were isolated by using a Ficoll gradient (Cedarlane); CNS homogenates were separated into neuronal and leukocyte populations by discontinuous density gradient centrifugation using isotonic Percoll (Amersham). For surface marker stainings, cells were incubated with fluorochrome-conjugated antibodies at the recommended dilution or with isotype control antibodies listed above for 20 min at 4°C. For intracellular cytokine staining, isolated leukocytes were stimulated with PMA (10 ng/ml)/ionomycin (1 µg/ml; Sigma-Aldrich) in the presence of Brefeldin A (10 µg/ml; Sigma-Aldrich) at 37°C for 6 h. The intracellular staining kit (eBioscience) was used to permeabilize and fix the cells before staining for Foxp3 and intracellular cytokines. Stained cells were analyzed by flow cytometry (FACSCelesta, Becton Dickinson).

Morphological analyses

Immunofluorescence stainings of thin sections (6 µm) were performed as described previously (Agrawal et al., 2006). Sections were examined using a Zeiss AxioImager equipped with epifluorescent optics or a Zeiss LSM 700 confocal microscope and documented using a Hamamatsu ORCA ER camera.

In vivo proliferation assays

Active EAE was induced in WT and *Tek-cre::Lama5*$^{-/-}$ mice. BrdU was injected i.p. twice at the peak of EAE (days 14 and 16 after immunization). Lymph nodes, spleen, blood, and CNS were removed 12 h after the last injection, and isolated CD45.2$^+$CD4$^+$ T cells were analyzed for BrdU incorporation by flow cytometry.

In vitro cell adhesion assay

In vitro cell adhesion assays were performed as previously described (Frieser et al., 1996) using colorimetric analysis of lysosomal hexosaminidase (OD_{405}; Landegren, 1984) to quantitate the number of adherent cells. 96-well plates (Nunc, MaxiSorp) were coated overnight at 4°C with BSA and laminin 111, 411, or 511 (1–10 µg/ml diluted in PBS), washed twice with PBS, and blocked with 1% BSA in PBS at 37°C for 1 h. CD4$^+$ T cells from EAE mice (day 10–12 after active immunization) were isolated from spleens and lymph nodes using anti-CD4–coated MACS beads (Miltenyi Biotec) and adjusted to 1.5×10^6 cells/ml in cell attachment buffer (DMEM, 0.5% cell-grade BSA, and 10 mM Hepes). 1.5×10^5 CD4$^+$ T cells were added per well and incubated at 37°C/5% CO_2 for indicated times, and absolute numbers of adherent cells were measured using the lysosomal hexosaminidase assay (Landegren, 1984). Absolute binding to BSA denoted nonspecific binding and was subtracted from values measured on laminin substrates, and percentages of adherent cells were determined (total bound number/total cell number applied). Binding in the absence of inhibitory antibody was set to 100%, and percentage inhibition was calculated.

Inhibition studies to investigate the receptors responsible for the adhesion to different substrates involved preincubation of cells on ice for 20 min with 20 µg/ml function blocking antibodies or peptides (10–100 µM for RGD peptides) before addition to protein-coated 96-well plates. Inhibition experiments were performed using a single concentration of extracellular matrix protein (20 µg/ml) in the presence of the inhibitors.

Optical tweezer experiments

To measure strengths of adhesion, CD4$^+$ T cells were seeded onto 0.1 or 1 µg/ml laminin 411 or 511 or BSA and incubated at 37°C for 60 min. Cells were visualized using an inverse fluorescence microscope (Eclipse Ti, Nikon) under a 100× oil-immersion objective (numerical aperture = 1.49). The microscope was equipped with a 2.5-W neodymium-doped yttrium orthovanadate laser operating at a wavelength of 1,064 nm, allowing manipulation of cells with low photodamage and a phase-only spatial light modulator (SLM; Holoeye, Pluto) with a resolution of 1,920 × 1,080 pixels. The SLM, working in reflection geometry, is imaged onto the back aperture of the microscope's objective via a telescope, formed by lenses L2 and L3. A dichroic mirror is used to couple the laser beam into the microscope and, together with a filter (stopband at 1,064 nm), it separates the laser beam path from the observation path. The SLM displays a sequence of holograms whose Fourier transform represents the desired trapping geometry. For hologram calculation, a LabView

program was used. This system allows independent control of multiple traps interactively. Cells were optically trapped and were actively pulled from the substrate using a constant force of 70 pN. Measurement of cell displacement is inversely correlated to the strength of adhesion to the substrate. Images were acquired by a Photonfocus high-speed camera (MV2-D1280-640-CL).

Transmigration assays

Transwell filters (5 µm, Costar) were coated overnight at 4°C with 20 µg/ml purified laminin 411, laminin 511, recombinant laminin 511 domain IVa, recombinant mini-laminin 511, or laminin 111 as a control substrate. Filters were blocked with 1% BSA in PBS for 1 h at 37°C, and 5 × 10^5 $CD4^+$ T cells isolated from EAE mice in attachment buffer were added to the upper chamber. Transmigration was induced by adding 500 ng/ml CCL21 (Promokine) to the bottom chamber. After 6 h at 37°C, the transmigrated cells were counted and expressed as a percentage of total cells added to the upper chamber. In some cases, $CD4^+$ T cells were pretreated with function blocking anti-integrin antibodies or peptides, as described above, before adding to the upper chamber.

2D chemotaxis assays

$CD4^+$ T cells isolated from EAE mice were suspended in cell attachment buffer and 2.5 × 10^3 cells were seeded per 70 µm channel of µ-slide Chemotaxis Chamber (Ibidi); channels were precoated with 20 µg/ml laminin 411 or 511 or BSA. The narrow channel (observation area) separates two ∼40 µl reservoirs. A final concentration of 500 ng/ml CCL21 was added to one of the reservoirs together with 0.003% Patentblau V (Chroma Gesellschaft), and the cells were imaged by phase-contrast microscopy (Zeiss Axiovert 200M). The Patentblau V was used as a visual indicator of gradient formation and did not affect cell migration or cell survival. Images were captured every 2 min for 2 h, and cell migration tracks between 45 and 90 min were analyzed in ImageJ (National Institutes of Health) using a manual tracking plugin and the chemotaxis and migration tool from Ibidi. Between 20 and 25 randomly selected cells were manually tracked in each chemotaxis experiment and expressed as a spider diagram.

In vitro Th1/Th17 cell polarization

96-well plates were coated overnight at 4°C with 100 µl of 20 µg/ml laminin 411 or 511 or PBS as control. $CD4^+$ T cells were isolated from draining lymph nodes of WT mice on day 12 after EAE induction using magnetic beads (Miltenyi Biotec), and 0.5 × 10^6 cells were added to the laminin-coated or uncoated plates together with WT $CD11c^+$ dendritic cells (0.25 × 10^6) and 20 µg/ml $MOG_{35–55}$. Cells were cultured in the presence of 20 µg/ml IL-12 (Miltenyi Biotec) to induce Th1 cell differentiation, or in the presence of 10 µg/ml anti-IFN-γ (BioLegend, clone R4-6A2), 20 ng/ml IL-6 (Miltenyi Biotec), and 10 ng/ml TGF-β (R&D Systems) to induce Th17 differentiation. After 4 d, for the last 4 h of culture, cells were stimulated with PMA (10 ng/ml) and ionomycin (1 µg/ml), and Brefeldin A (10 µg/ml) was added to permit intracellular cytokine staining with anti-IL-17A (eBioscience, clone eBio17B7) and anti-INF-γ (BioLegend, clone XMG1). Th1 and Th17 cells as percentages of total cells were determined by using a FACSCelesta flow cytometer (Becton Dickinson).

qPCR for expression of T cell pathogenic markers

Integrin $\alpha6^{high}\alpha v^{low}$ and integrin $\alpha6^{high}\alpha v^{high}$ $CD4^+$ T cells were sorted from CNS extracts by flow cytometry (FACS-ARIA, Bectin Dickensen) and analyzed by qPCR for the following markers of different Th17 populations: *Il10*, *Il17a*, *Ifng*, *Gpr65*, *Plzp*, *Toso*, and *Cd5l* (Gaublomme et al., 2015). Total RNA from 1 × 10^5 sorted cells was prepared using the RNeasy kit (Qiagen), and cDNAs were generated (Omniscript RT Kit, Qiagen). qPCR was performed using Brilliant SYBR Green QPCR Master Mix (Agilent Technologies). qPCR was performed with an Applied Biosystems PRISM 7300 Sequence Detection System. Relative quantification was performed using the comparative threshold (CT) method, in which the amount of the target is normalized to the GAPDH reference and relative to a calibrator, given by $2^{-\Delta CT}$. Three to five biological replicates were used for each point investigated.

Statistical analyses

The data were analyzed by GraphPad Prism 7.0 software and are presented as means ± SEM or SD as indicated. Significance of cell numbers was analyzed with a Mann–Whitney *U* test. Kaplan-Meier survival analysis and log-rank test were used to analyze mice survival and incidence. Values of $P < 0.05$ were considered significant.

Online supplemental material

Fig. S1 shows integrin profiles and MCAM on $Itga6^{-/-}$ and $Itgav^{-/-}$ $CD4^+$ T cells and WT controls, and integrin α6, αv, and β1 levels on $CD4^+$ T cells in brain, spinal cord, spleen, and lymph node under naive and EAE conditions. Fig. S2 shows concentration-dependent, saturable binding of WT encephalitogenic $CD4^+$ T cells to mini-laminin 511 and laminin 511 domain IVa, and transmigration of WT encephalitogenic $CD4^+$ T cells across mini-laminin 511, laminin 511 domain IVa, and laminin 411. Fig. S3 shows quantification of immune cells, including Th1 and Th17 $CD4^+$ T cells, in spinal cords of WT and *Tek-cre::Lama5*$^{-/-}$ mice at peak EAE, as well as in vivo proliferation and migration of adoptively transferred encephalitogenic $CD4^+$ T cells in WT and *Tek-cre::Lama5*$^{-/-}$ mice, the corresponding clinical scores over a 40-d period, and quantification of transferred cells in the CNS and periphery.

Acknowledgments

We thank Reinhardt Fässler (Max-Planck Institute for Biochemistry, Martinsried, Germany) for the $Itgav^{floxed/floxed}$ mice; and Miriam Burmeister, Sigmund Budny, Melanie-Jane Hannocks, and Rupert Hallmann (Institute of Physiological Chemistry and Pathobiochemistry, University of Muenster, Muenster, Germany) for help with scoring of mice, purification of laminins and antibodies, and critical reading of the manuscript.

The work was supported by funding to L. Sorokin from the German Research Foundation (CRC1009 A02, TR128 B03, and EXE1003).

Author contributions: X. Zhang performed all EAE studies on *Tek-cre::Lama5*$^{-/-}$ and WT littermates, flow cytometry to quantify immune cell numbers, and many of the in vitro transmigration assays. Y. Wang contributed to the in vitro adhesion and migration assays. J. Song performed all in vivo and in vitro experiments with *Itgav*$^{-/-}$ cells and performed gene expression analyses of in vitro and in vivo Th17 cells. H. Gerwien developed and optimized the in vitro Th1 and Th17 differentiation assays and provided all such data shown in the manuscript. O. Chuquisana performed flow cytometry for expression of β1-integrins on WT and EAE T cells. A. Chashchina contributed to original Th1 and Th17 in vitro differentiation assays. C. Denz performed the optical tweezer experiments. L. Sorokin designed the projected, supervised all work, and wrote the manuscript.

Disclosures: The authors declare no competing interests exist.

Submitted: 19 July 2019
Revised: 31 January 2020
Accepted: 7 April 2020

References

Acharya, M., S. Mukhopadhyay, H. Païdassi, T. Jamil, C. Chow, S. Kissler, L.M. Stuart, R.O. Hynes, and A. Lacy-Hulbert. 2010. αv Integrin expression by DCs is required for Th17 cell differentiation and development of experimental autoimmune encephalomyelitis in mice. *J. Clin. Invest*. 120:4445–4452. https://doi.org/10.1172/JCI43796

Agrawal, S., P. Anderson, M. Durbeej, N. van Rooijen, F. Ivars, G. Opdenakker, and L.M. Sorokin. 2006. Dystroglycan is selectively cleaved at the parenchymal basement membrane at sites of leukocyte extravasation in experimental autoimmune encephalomyelitis. *J. Exp. Med*. 203: 1007–1019. https://doi.org/10.1084/jem.20051342

Bai, X.F., O. Li, Q. Zhou, H. Zhang, P.S. Joshi, X. Zheng, Y. Liu, Y. Wang, P. Zheng, and Y. Liu. 2004. CD24 controls expansion and persistence of autoreactive T cells in the central nervous system during experimental autoimmune encephalomyelitis. *J. Exp. Med*. 200:447–458. https://doi.org/10.1084/jem.20040131

Croxford, A.L., M. Lanzinger, F.J. Hartmann, B. Schreiner, F. Mair, P. Pelczar, B.E. Clausen, S. Jung, M. Greter, and B. Becher. 2015. The Cytokine GM-CSF Drives the Inflammatory Signature of CCR2+ Monocytes and Licenses Autoimmunity. *Immunity*. 43:502–514. https://doi.org/10.1016/j.immuni.2015.08.010

Dangerfield, J., K.Y. Larbi, M.T. Huang, A. Dewar, and S. Nourshargh. 2002. PECAM-1 (CD31) homophilic interaction up-regulates alpha6beta1 on transmigrated neutrophils in vivo and plays a functional role in the ability of alpha6 integrins to mediate leukocyte migration through the perivascular basement membrane. *J. Exp. Med*. 196:1201–1211. https://doi.org/10.1084/jem.20020324

Di Russo, J., A.L. Luik, L. Yousif, S. Budny, H. Oberleithner, V. Hofschröer, J. Klingauf, E. van Bavel, E.N. Bakker, P. Hellstrand, et al. 2017. Endothelial basement membrane laminin 511 is essential for shear stress response. *EMBO J*. 36:183–201. https://doi.org/10.15252/embj.201694756

Du, F., A.V. Garg, K. Kosar, S. Majumder, D.G. Kugler, G.H. Mir, M. Maggio, M. Henkel, A. Lacy-Hulbert, and M.J. McGeachy. 2016. Inflammatory Th17 Cells Express Integrin αvβ3 for Pathogenic Function. *Cell Rep*. 16: 1339–1351. https://doi.org/10.1016/j.celrep.2016.06.065

Durbeej, M.. 2010. Laminins. *Cell Tissue Res*. 339:259–268. https://doi.org/10.1007/s00441-009-0838-2

Flanagan, K., K. Fitzgerald, J. Baker, K. Regnstrom, S. Gardai, F. Bard, S. Mocci, P. Seto, M. You, C. Larochelle, et al. 2012. Laminin-411 is a vascular ligand for MCAM and facilitates TH17 cell entry into the CNS. *PLoS One*. 7. e40443. https://doi.org/10.1371/journal.pone.0040443

Frieser, M., R. Hallmann, S. Johansson, D. Vestweber, S.L. Goodman, and L. Sorokin. 1996. Mouse polymorphonuclear granulocyte binding to extracellular matrix molecules involves beta 1 integrins. *Eur. J. Immunol*. 26:3127–3136. https://doi.org/10.1002/eji.1830261245

Frieser, M., H. Nöckel, F. Pausch, C. Röder, A. Hahn, R. Deutzmann, and L.M. Sorokin. 1997. Cloning of the mouse laminin alpha 4 cDNA. Expression in a subset of endothelium. *Eur. J. Biochem*. 246:727–735. https://doi.org/10.1111/j.1432-1033.1997.t01-1-00727.x

Funk, S.D., M.H. Lin, and J.H. Miner. 2018. Alport syndrome and Pierson syndrome: Diseases of the glomerular basement membrane. *Matrix Biol*. 71–72:250–261. https://doi.org/10.1016/j.matbio.2018.04.008

García-Nieto, S., R.K. Johal, K.M. Shakesheff, M. Emara, P.J. Royer, D.Y. Chau, F. Shakib, and A.M. Ghaemmaghami. 2010. Laminin and fibronectin treatment leads to generation of dendritic cells with superior endocytic capacity. *PLoS One*. 5. e10123. https://doi.org/10.1371/journal.pone.0010123

Gaublomme, J.T., N. Yosef, Y. Lee, R.S. Gertner, L.V. Yang, C. Wu, P.P. Pandolfi, T. Mak, R. Satija, A.K. Shalek, et al. 2015. Single-Cell Genomics Unveils Critical Regulators of Th17 Cell Pathogenicity. *Cell*. 163: 1400–1412. https://doi.org/10.1016/j.cell.2015.11.009

Georges-Labouesse, E., N. Messaddeq, G. Yehia, L. Cadalbert, A. Dierich, and M. Le Meur. 1996. Absence of integrin alpha 6 leads to epidermolysis bullosa and neonatal death in mice. *Nat. Genet*. 13:370–373. https://doi.org/10.1038/ng0796-370

Hohenester, E., and P.D. Yurchenco. 2013. Laminins in basement membrane assembly. *Cell Adhes. Migr*. 7:56–63. https://doi.org/10.4161/cam.21831

Künneken, K., G. Pohlentz, A. Schmidt-Hederich, U. Odenthal, N. Smyth, J. Peter-Katalinic, P. Bruckner, and J.A. Eble. 2004. Recombinant human laminin-5 domains. Effects of heterotrimerization, proteolytic processing, and N-glycosylation on alpha3beta1 integrin binding. *J. Biol. Chem*. 279:5184–5193. https://doi.org/10.1074/jbc.M310424200

Landegren, U.. 1984. Measurement of cell numbers by means of the endogenous enzyme hexosaminidase. Applications to detection of lymphokines and cell surface antigens. *J. Immunol. Methods*. 67:379–388. https://doi.org/10.1016/0022-1759(84)90477-0

Lee, E.C., M.M. Lotz, G.D. Steele, Jr., and A.M. Mercurio. 1992. The integrin alpha 6 beta 4 is a laminin receptor. *J. Cell Biol*. 117:671–678. https://doi.org/10.1083/jcb.117.3.671

Lee, P.P., D.R. Fitzpatrick, C. Beard, H.K. Jessup, S. Lehar, K.W. Makar, M. Pérez-Melgosa, M.T. Sweetser, M.S. Schlissel, S. Nguyen, et al. 2001. A critical role for Dnmt1 and DNA methylation in T cell development, function, and survival. *Immunity*. 15:763–774. https://doi.org/10.1016/S1074-7613(01)00227-8

McCarty, J.H., A.A. Cook, and R.O. Hynes. 2005. An interaction between alphavbeta8 integrin and Band 4.1B via a highly conserved region of the Band 4.1 C-terminal domain. *Proc. Natl. Acad. Sci. USA*. 102:13479–13483. https://doi.org/10.1073/pnas.0506068102

Milner, R., and I.L. Campbell. 2002. The integrin family of cell adhesion molecules has multiple functions within the CNS. *J. Neurosci. Res*. 69: 286–291. https://doi.org/10.1002/jnr.10321

Miner, J.H., and P.D. Yurchenco. 2004. Laminin functions in tissue morphogenesis. *Annu. Rev. Cell Dev. Biol*. 20:255–284. https://doi.org/10.1146/annurev.cellbio.20.010403.094555

Miyazaki, T., S. Futaki, K. Hasegawa, M. Kawasaki, N. Sanzen, M. Hayashi, E. Kawase, K. Sekiguchi, N. Nakatsuji, and H. Suemori. 2008. Recombinant human laminin isoforms can support the undifferentiated growth of human embryonic stem cells. *Biochem. Biophys. Res. Commun*. 375: 27–32. https://doi.org/10.1016/j.bbrc.2008.07.111

Niessen, C.M., F. Hogervorst, L.H. Jaspars, A.A. de Melker, G.O. Delwel, E.H. Hulsman, I. Kuikman, and A. Sonnenberg. 1994. The alpha 6 beta 4 integrin is a receptor for both laminin and kalinin. *Exp. Cell Res*. 211: 360–367. https://doi.org/10.1006/excr.1994.1099

Nishiuchi, R., J. Takagi, M. Hayashi, H. Ido, Y. Yagi, N. Sanzen, T. Tsuji, M. Yamada, and K. Sekiguchi. 2006. Ligand-binding specificities of laminin-binding integrins: a comprehensive survey of laminin-integrin interactions using recombinant alpha3beta1, alpha6beta1, alpha7beta1 and alpha6beta4 integrins. *Matrix Biol*. 25:189–197. https://doi.org/10.1016/j.matbio.2005.12.001

Nyström, A., and L. Bruckner-Tuderman. 2019. Matrix molecules and skin biology. *Semin. Cell Dev. Biol*. 89:136–146. https://doi.org/10.1016/j.semcdb.2018.07.025

Overstreet, M.G., A. Gaylo, B.R. Angermann, A. Hughson, Y.M. Hyun, K. Lambert, M. Acharya, A.C. Billroth-Maclurg, A.F. Rosenberg, D.J. Topham, et al. 2013. Inflammation-induced interstitial migration of effector CD4$^+$ T cells is dependent on integrin αV. *Nat. Immunol*. 14: 949–958. https://doi.org/10.1038/ni.2682

Pallarola, D., A. Bochen, H. Boehm, F. Rechenmacher, T.R. Sobahi, J.P. Spatz, and H. Kessler. 2014. Interface Immobilization Chemistry of cRGD-based Peptides Regulates Integrin Mediated Cell Adhesion. *Adv. Funct. Mater*. 24:943–956. https://doi.org/10.1002/adfm.201302411

Ringelmann, B., C. Röder, R. Hallmann, M. Maley, M. Davies, M. Grounds, and L. Sorokin. 1999. Expression of laminin alpha1, alpha2, alpha4, and alpha5 chains, fibronectin, and tenascin-C in skeletal muscle of dystrophic 129ReJ dy/dy mice. *Exp. Cell Res.* 246:165–182. https://doi.org/10.1006/excr.1998.4244

Sasaki, T., and R. Timpl. 2001. Domain IVa of laminin alpha5 chain is cell-adhesive and binds beta1 and alphaVbeta3 integrins through Arg-Gly-Asp. *FEBS Lett.* 509:181–185. https://doi.org/10.1016/S0014-5793(01)03167-2

Schöttelndreier, H., B.V. Potter, G.W. Mayr, and A.H. Guse. 2001. Mechanisms involved in alpha6beta1-integrin-mediated Ca(2+) signalling. *Cell. Signal.* 13:895–899. https://doi.org/10.1016/S0898-6568(01)00225-X

Seder, R.A., R. Gazzinelli, A. Sher, and W.E. Paul. 1993. Interleukin 12 acts directly on CD4+ T cells to enhance priming for interferon gamma production and diminishes interleukin 4 inhibition of such priming. *Proc. Natl. Acad. Sci. USA.* 90:10188–10192. https://doi.org/10.1073/pnas.90.21.10188

Shaw, L.M., J.M. Messier, and A.M. Mercurio. 1990. The activation dependent adhesion of macrophages to laminin involves cytoskeletal anchoring and phosphorylation of the alpha 6 beta 1 integrin. *J. Cell Biol.* 110:2167–2174. https://doi.org/10.1083/jcb.110.6.2167

Sixt, M., B. Engelhardt, F. Pausch, R. Hallmann, O. Wendler, and L.M. Sorokin. 2001a. Endothelial cell laminin isoforms, laminins 8 and 10, play decisive roles in T cell recruitment across the blood-brain barrier in experimental autoimmune encephalomyelitis. *J. Cell Biol.* 153:933–946. https://doi.org/10.1083/jcb.153.5.933

Sixt, M., R. Hallmann, O. Wendler, K. Scharffetter-Kochanek, and L.M. Sorokin. 2001b. Cell adhesion and migration properties of beta 2-integrin negative polymorphonuclear granulocytes on defined extracellular matrix molecules. Relevance for leukocyte extravasation. *J. Biol. Chem.* 276:18878–18887. https://doi.org/10.1074/jbc.M010898200

Song, J., Z. Lokmic, T. Lämmermann, J. Rolf, C. Wu, X. Zhang, R. Hallmann, M.J. Hannocks, N. Horn, M.A. Ruegg, et al. 2013. Extracellular matrix of secondary lymphoid organs impacts on B-cell fate and survival. *Proc. Natl. Acad. Sci. USA.* 110:E2915–E2924. https://doi.org/10.1073/pnas.1218131110

Song, J., C. Wu, E. Korpos, X. Zhang, S.M. Agrawal, Y. Wang, C. Faber, M. Schäfers, H. Körner, G. Opdenakker, et al. 2015. Focal MMP-2 and MMP-9 activity at the blood-brain barrier promotes chemokine-induced leukocyte migration. *Cell Rep.* 10:1040–1054. https://doi.org/10.1016/j.celrep.2015.01.037

Song, J., X. Zhang, K. Buscher, Y. Wang, H. Wang, J. Di Russo, L. Li, S. Lütke-Enking, A. Zarbock, A. Stadtmann, et al. 2017. Endothelial Basement Membrane Laminin 511 Contributes to Endothelial Junctional Tightness and Thereby Inhibits Leukocyte Transmigration. *Cell Rep.* 18:1256–1269. https://doi.org/10.1016/j.celrep.2016.12.092

Sorokin, L.. 2010. The impact of the extracellular matrix on inflammation. *Nat. Rev. Immunol.* 10:712–723. https://doi.org/10.1038/nri2852

Sorokin, L.M., F. Pausch, M. Frieser, S. Kröger, E. Ohage, and R. Deutzmann. 1997. Developmental regulation of the laminin alpha5 chain suggests a role in epithelial and endothelial cell maturation. *Dev. Biol.* 189:285–300. https://doi.org/10.1006/dbio.1997.8668

Thyboll, J., J. Kortesmaa, R. Cao, R. Soininen, L. Wang, A. Iivanainen, L. Sorokin, M. Risling, Y. Cao, and K. Tryggvason. 2002. Deletion of the laminin alpha4 chain leads to impaired microvessel maturation. *Mol. Cell. Biol.* 22:1194–1202. https://doi.org/10.1128/MCB.22.4.1194-1202.2002

Tözeren, A., H.K. Kleinman, S. Wu, A.M. Mercurio, and S.W. Byers. 1994. Integrin alpha 6 beta 4 mediates dynamic interactions with laminin. *J. Cell Sci.* 107:3153–3163.

Tran, E.H., K. Hoekstra, N. van Rooijen, C.D. Dijkstra, and T. Owens. 1998. Immune invasion of the central nervous system parenchyma and experimental allergic encephalomyelitis, but not leukocyte extravasation from blood, are prevented in macrophage-depleted mice. *J. Immunol.* 161:3767–3775.

Veldhoen, M., R.J. Hocking, C.J. Atkins, R.M. Locksley, and B. Stockinger. 2006. TGFbeta in the context of an inflammatory cytokine milieu supports de novo differentiation of IL-17-producing T cells. *Immunity.* 24:179–189. https://doi.org/10.1016/j.immuni.2006.01.001

Wang, C., N. Yosef, J. Gaublomme, C. Wu, Y. Lee, C.B. Clish, J. Kaminski, S. Xiao, G. Meyer Zu Horste, M. Pawlak, et al. 2015. CD5L/AIM Regulates Lipid Biosynthesis and Restrains Th17 Cell Pathogenicity. *Cell.* 163:1413–1427. https://doi.org/10.1016/j.cell.2015.10.068

Wang, S., M.B. Voisin, K.Y. Larbi, J. Dangerfield, C. Scheiermann, M. Tran, P.H. Maxwell, L. Sorokin, and S. Nourshargh. 2006. Venular basement membranes contain specific matrix protein low expression regions that act as exit points for emigrating neutrophils. *J. Exp. Med.* 203:1519–1532. https://doi.org/10.1084/jem.20051210

Woodfin, A., M.B. Voisin, M. Beyrau, B. Colom, D. Caille, F.M. Diapouli, G.B. Nash, T. Chavakis, S.M. Albelda, G.E. Rainger, et al. 2011. The junctional adhesion molecule JAM-C regulates polarized transendothelial migration of neutrophils in vivo. *Nat. Immunol.* 12:761–769. https://doi.org/10.1038/ni.2062

Wu, C., F. Ivars, P. Anderson, R. Hallmann, D. Vestweber, P. Nilsson, H. Robenek, K. Tryggvason, J. Song, E. Korpos, et al. 2009. Endothelial basement membrane laminin alpha5 selectively inhibits T lymphocyte extravasation into the brain. *Nat. Med.* 15:519–527. https://doi.org/10.1038/nm.1957

Yurchenco, P.D., K.K. McKee, J.R. Reinhard, and M.A. Rüegg. 2018. Laminin-deficient muscular dystrophy: Molecular pathogenesis and structural repair strategies. *Matrix Biol.* 71–72:174–187. https://doi.org/10.1016/j.matbio.2017.11.009

Supplemental material

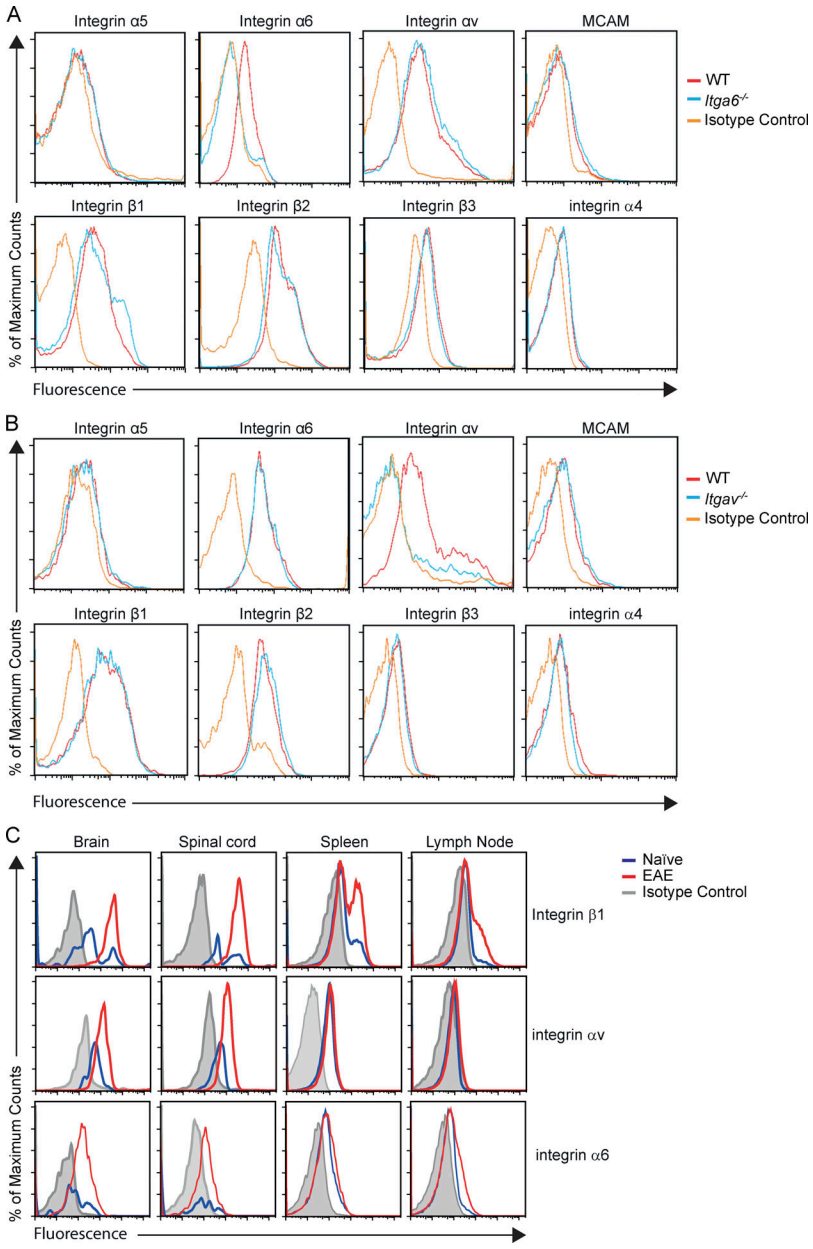

Figure S1. **Flow cytometry for integrins and MCAM expression levels on CD4⁺ T cells in naive and EAE conditions. (A and B)** Representative flow cytometry of integrin profiles and MCAM on *Itga6*$^{-/-}$ (A) and *Itgav*$^{-/-}$ (B) CD4⁺ T cells compared with corresponding WT and isotype controls (Iso-ctrl). Data are representative of three independent experiments, *n* = 3–4 mice/group/experiment. **(C)** Representative flow cytometry of integrin α6, αv, and β1 levels on CD4 T cells in brain, spinal cord, spleen, and lymph node under naive and EAE conditions. Data are representative of three independent experiments; *n* = 3–4 mice/group/experiment. Very few cells are present in the brain and spinal cord under naive conditions, resulting in the low maximum counts.

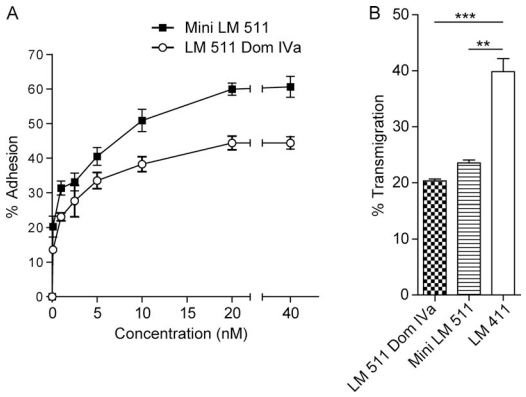

Figure S2. **Characterization of mini laminin 511 and laminin 511 domain IVa for use in adhesion and transmigration assays. (A)** Concentration-dependent, saturable binding of WT encephalitogenic CD4⁺ T cells to mini-laminin 511 and laminin 511 domain IVa. **(B)** Transmigration of WT encephalitogenic CD4⁺ T cells across mini-laminin 511, laminin 511 domain IVa, and laminin 411. Data in A and B are expressed as a percentage of total cells added and are means ± SD of five experiments, *n* = 3 replicates/group/experiment. Statistical analysis used a Mann–Whitney *U* test; **, P < 0.01; ***, P < 0.001.

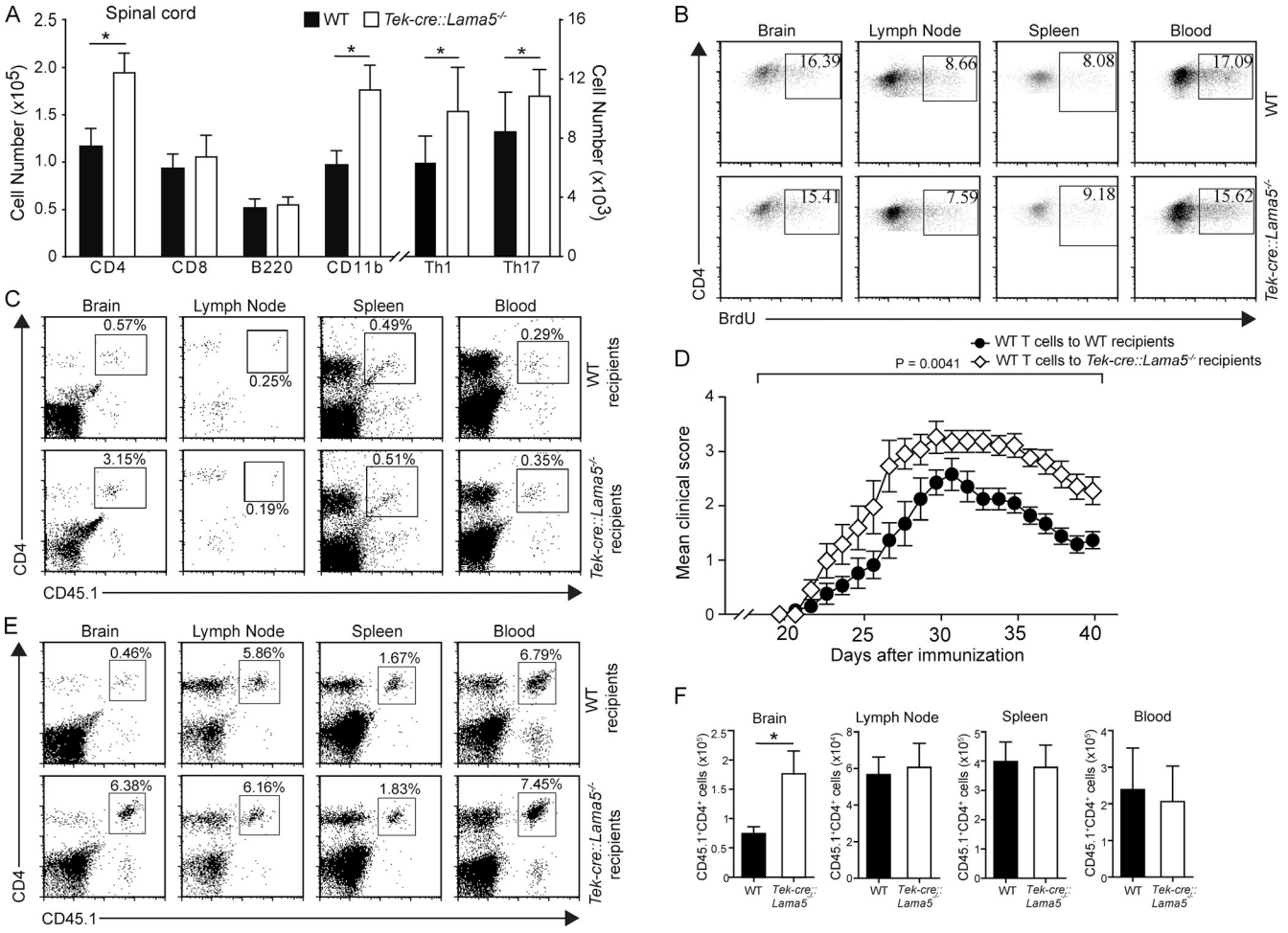

Figure S3. **Quantification of immune cells in spinal cords of WT and *Tek-cre::Lama5*$^{-/-}$ mice at peak EAE and in vivo proliferation and migration of adoptively transferred encephalitogenic CD4$^+$ T cells in WT and *Tek-cre::Lama5*$^{-/-}$ mice with corresponding clinical scores over a 40 d period and quantification of transferred cells in the CNS and periphery. (A)** Quantification of flow cytometry analyses of CD8$^+$ and CD4$^+$ T cells, B220$^+$ B cells, CD11b$^+$ macrophages, and Th1 and Th17 CD4$^+$ T cells in spinal cords of WT and Tek-cre::*Lama5*$^{-/-}$ mice at peak EAE. Data are means ± SD of three experiments, n = 5 mice/group/experiment. Statistical analysis used a Mann–Whitney U test; *, P < 0.05. **(B)** Representative flow cytometry of three experiments of BrdU$^+$ CD4$^+$ T cells in the brain, spleen, lymph node, and blood of WT and *Tek-cre::Lama5*$^{-/-}$ mice at peak EAE. **(C)** WT CD45.1$^+$ CD4$^+$ T cells were adoptively transferred to CD45.2$^+$ *Tek-cre::Lama5*$^{-/-}$ and WT recipients and analyzed at day 3 by flow cytometry for infiltrating CD45.1$^+$ CD4 T cells; representative flow cytometry of three experiments is shown. **(D)** The same adoptive transfer experiments were performed over a 40-d period, and mean clinical scores were measured. Data shown are means ± SD of two experiments, n = 7 mice/group. Statistical analysis used a Mann–Whitney U test; P value is shown. **(E and F)** Corresponding representative flow cytometry of adoptively transferred WT CD45.1$^+$ CD4$^+$ T cells in the brain, lymph node, spleen, and blood at peak EAE (E) and quantification of the data (F). Data are means ± SD of three experiments, n = 9 mice/group. Statistical analysis used a Mann–Whitney U test; *, P < 0.05.